PERIODICLLY BEHAVED LONGITUDINAL VORTICES DOWNSTREAM OF AN ACTIVE VORTEX GENERATORS (RESPONSE OF FULL COMPONENTS OF TURBULENT PROPERTIES)

Takaaki Shizawa
Department of Mechanics and Systems Design
Tokyo University of Science, Suwa
Chino, Nagano, 391-0292, Japan
shizawa@rs.suwa.tus.ac.jp

Shinya Endo
Mizushima Oil Refinery
Japan Energy Co.
Kurashiki, Okayama, 712-8588, Japan
rwjsn107@ybb.ne.jp

Masahiro Nakajima
Tochigi R&D Center
Honda R&D Co. Ltd.
Haga, Tochigi, 321-3393, Japan
masahiro_nakajima@n.t.rd.honda.co.jp

Shinji Honami
Department of Mechanical Engineering
Tokyo University of Science
Shinjuku, Tokyo, 162-8601, Japan
honamis@rs.kagu.tus.ac.jp

ABSTRACT

This paper is focused on the phase averaged characteristics of longitudinal vortices (*LV*) downstream of a pair of active vortex generators (*AVG*) with common flow up configuration. A smart control of turbulent shear flow on a flat surface is one of the most challenging projects. It is important to understand the periodically behaved interacting processes between turbulent boundary layer and *LV*. The objective of this paper is to experimentally make clear the response of full components of Reynolds stresses and triple-products of periodically behaved *LV* submerged in a two-dimensional turbulent boundary layer to the height of *AVG*. The 'high velocity tongue' of upwash side of the *LV* responds to the same manner as the height of *AVG* by time depended characteristics of negative peak of Reynolds stress $-\overline{u'v'}$.

INTRODUCTION

An active control of turbulent shear flow on a wing of aircraft, an air intake and a diffuser of jet engine is one of the currently most challenging projects. One of the boundary layer control methods is to use a vortex generator. It is important to establish smart control methods based on the information of transient interacting processes of *LV* and turbulent boundary layer. Also, the other interests are to understand the response of *LV* to the height of *AVG*.

A number of investigators have been concerned with the problems of formation and development of three-dimensional vortical structure in turbulent shear flow. One of the research works after 1980's is the separation control or boundary layer manipulation by vortex generators. The representative research work by Pauley and Eaton (1988a, b) is the compilation of static vortex generator on turbulent boundary layer. These papers are focused on the common-flow characteristics between the vortex generators pair. Shizawa et al. (1999) shows another application of *LV* to control a horseshoe vortex by common-flow up configuration of a pair of vortex generators. Littell and Eaton (1991) investigate the time depended characteristics of *LV* downstream of a vortex generator pitched to angle of attack. Shizawa et al. (2003) present the phase averaged behavior of 'high velocity tongue' at upwash side of the *LV*. Shizawa and Mizusaki (2004) present the rapid response of phase averaged mean velocity at the early-stage of up-phase to the height of *AVG*.

This paper is focused on the conditional averaged characteristics of full components of turbulent properties and the interacting processes of periodically behaved *LV* by newly developed rotating *X*-array hot-wire anemometer. Time depended characteristics of *LV* downstream of a pair of *AVG* with common-flow up configuration are investigated experimentally. The transient response of *LV* to the height of *AVG* is also discussed.

EXPERIMENTAL SETUP AND METHOD

Experimental Setup. A return type of wind tunnel with a rectangular cross section of 1,500 mm in length, 720 mm in width and 130 mm in height is used. The origin of the coordinate system is selected at the mid-cord of the *AVG* as shown in Figure 1. The free–stream velocity at the upstream reference point is U_r = 17.2 m/s within 1 % error and the turbulent intensity is 0.5 %. The boundary layer thickness is δ = 20.6 mm and the momentum thickness Reynolds number is Re_θ = 2,600.

Figure 2 shows the schematic drawing of a circular wing lip type of *AVG*. The backrush–less spur gear is 60 mm in diameter with modulus of 0.5. The *AVG* is actuated up and down by changing its height periodically at ω = 21.6 rad/s by means of a high–speed stepping motor. The location and the speed of *AVG* are detected by a photo micro–sensor. A pair of this system is attached on the test surface at common–flow up configuration and the angle of yaw is set at 18 degree. The *AVG* pair is highly synchronized each other and the delay–time between *AVG* is less than 0.3 ms. Pulse is generated every 3.125 ms and

the period of up– and down–phase is 50 ms as shown in Figure 3. The steady-phase is set to obtain the transient characteristics of longitudinal vortices. The maximum height of *AVG* is H = 17.23 mm. The spacing of the *AVG* which is measured at the bisector of each *AVG* is S = 40 mm.

Rotating *X*-array Hot-Wire. The full components of turbulent properties are measured by a newly developed rotating *X*–array hot–wire anemometer. The shear stress $\overline{v'w'}$ which could not measure using conventional *X*-array hot-wire is reduced from the two rotating positions subscript 3 and 4 of the rotating *X*-array hot-wire and other known five components of Reynolds stress neglecting mean velocity components V and W proposed by Pauley and Eaton (1988).

$$\overline{v'w'} = \frac{F_3 - F_4 - (D_1^2 - D_3^2)\overline{u'^2} - (D_2^2 - D_4^2)(\overline{v'^2} + \overline{w'^2})}{2(D_2^2 + D_4^2)} - \frac{2(D_1D_2 - D_3D_4)\overline{u'v'} + 2(D_1D_2 + D_3D_4)\overline{u'w'}}{2(D_2^2 + D_4^2)} \quad (1)$$

The following relations are used to determine.

$$F_3 = \overline{\{(u_{3,1} - \overline{u_{3,1}}) - (u_{3,2} - \overline{u_{3,2}})\}^2}$$

$$F_4 = \overline{\{(u_{4,1} - \overline{u_{4,1}}) - (u_{4,2} - \overline{u_{4,2}})\}^2}$$

$$D_1 = C_{3,1} - C_{3,2}, \qquad D_2 = \frac{\sqrt{2}}{2}\left(\frac{S_{3,1}}{C_{3,1}} - \frac{S_{3,2}}{C_{3,2}}\right)$$

$$D_3 = C_{4,1} - C_{4,2}, \qquad D_4 = \frac{\sqrt{2}}{2}\left(\frac{S_{4,1}}{C_{4,1}} - \frac{S_{4,2}}{C_{4,2}}\right)$$

$$S_{i,j} = \sin\psi_{i,j} \qquad C_{i,j} = \cos\psi_{i,j}$$

i : *position* $\qquad$ j : *wire*

Since the measurements in these two planes were not made at the same time, only time averaged quantities could be used.

The stress in the probe coordinate system is transformed into the tunnel coordinate system using following relation.

$$\overline{v'w'}\big|_w = \overline{v'w'}\cos\gamma - \overline{u'v'}\sin\gamma \quad (2)$$

where γ is the yaw angle between hot-wire tip and the tunnel centerline.

The hot-wire probe has the sensing elements of tungsten wire of d = 3 μm in diameter, l = 0.84 mm in length. The spacing of each sensing element is set at 0.5 mm. The rotating *X*–array hot–wire anemometer is designed using a miniature stepping motor (CANON Electronic Inc., *CAM*39) as shown in Figure 4. Phase averaged velocity data over each 2048 samples are averaged at the sampling rate of 5 kHz by constant temperature hot-wire anemometer (DANTEC, StreamLine). The uncertainty analysis for mean velocity by the rotating *X*–array hot–wire anemometer is 3.0 % to the free stream velocity, 8.0 % for turbulent intensity and 15.0 % for Reynolds shear stress $-\overline{v'w'}$.

RESULTS AND DISCUSSIONS

Turbulent Properties. Among the turbulent properties, the Reynolds primary shear stress $-\overline{u'v'}$ is the most important. The secondary shear stress $-\overline{v'w'}$ is particularly important in the analysis of streamwise vortices because of its importance in the streamwise vorticity transport equation. The other important turbulent properties are the total turbulent stress and anisotropy term of the normal stresses.

Figure 5(a) presents the phase averaged Reynolds shear stress $-\overline{u'v'}$ contours in case of final-stage of up-phase and Figure 5(b) shows the contours in case of early-stage of down-phase. The solid contours present the positive value of $-\overline{u'v'}$ and the dotted contours present the negative value. The center location of *LV* at the steady-phase deduced from V = W = 0 m/s is Y/S = 0.38 and Z/S = 0.31.

The negative region which means the region of reversed velocity gradient in $\partial U/\partial Y$ is observed beneath and up-wash side of the *LV*. The region corresponds to the 'high velocity tongue' where the high velocity fluid penetrates beneath the *LV* and shifts up at upwash side. The negative contours firstly observed at 25 ms and lasted after 139 ms. Positive contours present two peaks. One is the top and the other is the vicinity of the center of *LV*. The rapid response to the height of *AVG* is observed at early-stage of up-phase but the negative region is still developed after the *AVG* reaches the top dead–end of 55 ms. The slow response is observed at early-stage of down-phase as comparison with the contours at 31 ms and 121 ms. Positive and negative contours both still show the large domain at 121 ms.

Figure 6 shows the phase averaged $-\overline{v'w'}$ contours in case of final-stage of up-phase and early-stage of down-phase. The negative region corresponds to the region of reversed velocity gradient in $\partial W/\partial Y$. The rapid response of $-\overline{v'w'}$ is observed in case of final-stage of up-phase. The contours present almost the same at 49 ms and 55 ms. The slow response is observed in case of final–stage of up–phase of 133 ms. Positive contours still present the core region at upwash side and vicinity of the center of the *LV*.

Response of Turbulent Properties. Figure 7 presents the response of peak value of turbulent properties to the height of *AVG*. Figure 7(a) shows the turbulent kinetic energy normalized by the peak value at steady-phase. The rapid response is observed at final-stage of up-phase and slow response is observed at early-stage of down-phase as shown in Shizawa et al. (2003).

Figure 7(b) represents the response of Reynolds shear stress $-\overline{u'v'}$. Solid circle presents the positive peak and open circle presents the negative peak. The rapid response of positive peak is observed in case of final-stage of up-phase. The peak value is increased before the *AVG* reaches *TDE* and is decreased at steady-phase. In case of down-phase, positive peak maintains the value at steady-phase. The location of negative peak corresponds to the core of high velocity tongue and the peak value is

increased as the same manner as the height of *AVG* in case of up-phase. Also the same response of $-\overline{u'v'}$ to the height of *AVG* is observed at down-phase.

Figure 7(c) presents the response of positive and negative peak value of $-\overline{v'w'}$. Rapid response of positive peak is observed in case of final-stage of up-phase. The peak value is decreased at steady-phase and increased again before the start of down-phase. On the other hand, negative peak is increased as the same manner as the height of *AVG* in case of up-phase and is changed little at steady-phase. The peak maintains almost the same value in case of early-stage of down-phase.

It is found that the time depended characteristics of core of the high velocity tongue follow the height of *AVG* as the results of the change of negative peak of Reynolds shear stress $-\overline{u'v'}$ and $-\overline{v'w'}$ in case of up-phase. Also, the response of core follows the height of *AVG* as the profile of negative peak of $-\overline{u'v'}$ in case of down-phase. On the other hand, the slow response of downwash motion of the *LV* to the height of *AGV* is observed in case of down-phase. Because the negative peak of $-\overline{v'w'}$ maintains constant at downwash side of the *LV*.

Characteristics of Total Turbulent Stress. The primary shear stress $-\overline{u'v'}$ and secondary shear stress $-\overline{v'w'}$ can be combined to obtain the total turbulent stress τ in plane parallel to the wall defined as equation (3).

$$\tau = \sqrt{(\overline{u'v'})^2 + (\overline{v'w'})^2} \qquad (3)$$

Figure 8 presents the phase averaged contours of total turbulent stress in case of early-stage of up-phase. The skewed contours are firstly observed close to the wall at 13 ms. The stress is increased as the lapse of time at the down-wash side of the *LV*. Two peaks of the stress at the down-wash side are observed after 31 ms and the value at the top of *LV* shows the higher value. In case of final-stage of up-phase, the peak at top and vicinity of the center of the *LV* shows larger value after 49 ms.

Characteristics of Anisotropy of Normal Stresses. The anisotropy term defined as $\overline{v'^2} - \overline{w'^2}$ produces streamwise vorticity if inhomogeneity of the normal stress anisotropy exists. Figure 9 shows the term in case of final-stage of up-phase. The effects of anisotropy of the stress are firstly observed at 25 ms. The effects are presented at the vicinity of the center of the *LV* and at the high velocity tongue. The profile distributes symmetrically into four quadrants about an 'X' through the center of the *LV* after 37 ms. The production of the vorticity at this mechanism is expected larger at the top of the *LV* in case of early-stage of up-phase. The vortex is dissipated at the same order at both downwash and upwash side of the *LV* .

Characteristics of Triple-Products. Figure 10 presents the contours of phase averaged triple-products $\overline{u'v'^2}$ profile at final–stage of up–phase. This term is to determine the diffusion of the primary shear stress $-\overline{u'v'}$ by turbulent velocity *v'*. The positive value is observed at the center of the *LV*. The negative value is firstly observed at 31 ms at the corresponding location of high velocity tongue. The location shifts away from the wall at 55 ms. Slow response of the triple-products to the height of *AVG* is observed in this case.

Figure 11 presents the contours of triple-products $\overline{v'^2 w'}$. The effects are firstly observed at 19 ms. The negative region is observed at the top of the *LV* and moved toward the downwash side of the *LV*. Several negative peaks are observed after 31 ms. The other negative region is observed at the corresponding location of high velocity tongue after 37 ms. The positive region develops at the center of *LV* and at the symmetry plane of *LV* pair including *Z/S* = 0. The higher peak of the product is observed at the up-phase of 25 ms to 31 ms. Positive peak of center of the *LV* is decreased at steady-phase. On the other hand, the peak at the symmetry plane of the *LV* pair is increased as the lapse of time.

CONCLUSIONS

The periodically behaved flowfield of *LV* generated downstream of the *AVG* pair with common-flow up configuration is investigated.

1. The response of Reynolds shear stress $-\overline{u'v'}$ and $-\overline{v'w'}$ to the height of *AVG* is made clear by newly developed rotating *X*-array hot-wire anemometer.
2. The time depended characteristics of high velocity tongue follow the height of *AVG* in case of up-phase as the results of the change of negative peak of Reynolds shear stress $-\overline{u'v'}$ and $-\overline{v'w'}$.
3. The response of downwash motion of the *LV* to the height of *AGV* is slow, since the large negative peak of $-\overline{v'w'}$ is maintained constant at downwash side of the *LV* in case of down-phase.
4. Two peaks of the total turbulent stress at the downwash side of *LV* are observed. The peak at the top of the *LV* shows the higher value in case of up-phase. The total turbulent stress at the vicinity of center and top of *LV* shows the larger value in case of steady-phase.
5. Slow response of the triple-products $\overline{u'v'^2}$ to the height of *AVG* is observed in case of final-stage of up-phase. The positive region of $\overline{v'^2 w'}$ is developed at the center of *LV* and at the symmetric plane of *LV* pair in case of up-phase.

ACKNOWLEDGEMENTS

The direct contributions of Mr. M. Hirase, Mr. K. Ohta, and Mr. T. Miyamoto at Tokyo Univ. of Science in conducting the experiments and interpreting the results made this study possible. The authors gratefully acknowledge the technical support of Mr. A. Kurosawa at Canon Electronics Inc. in designing and assembling the rotating *X*-array hot-wire anemometer.

REFERENCES

Littell, H. S., and Eaton, J. K., 1991, "Unsteady Flowfield Behind a Vortex Generator Rapidly Pitched to Angle of Attack ," AIAA J. Vol. 29 – 4, pp. 577-584.

Pauley, W. R., and Eaton, J. K., 1988a, "Experimental Study of the Development of Longitudinal Vortex Pairs Embedded in a Turbulent Boundary Layer," AIAA J., Vol. 26 – 7, pp. 816 – 823.

Pauley, W. R., and Eaton, J. K., 1988b, "The Fluid Dynamics and Heat Transfer Effects of Streamwise Vortices Embedded in a Turbulent Boundary Layer," Stanford Univ. Report MD-51, pp. 1 – 343.

Shizawa, T. et al., 1999, "Characteristics of Interacting Process with Horseshoe Vortex and Longitudinal Vortex," Proc. of Turbulence and Shear Flow Phenomena, First International Symposium, pp. 817 – 822.

Shizawa, T. et al., 2003, "Periodic Behavior of Longitudinal Vortices Downstream of an Active Vortex Generators (Phase-Averaged Velocity Response)", Proc. of Turbulent Shear Flows and Phenomena, Third International Symposium, Ⅱ, pp. 863 – 868.

Shizawa, T., and Mizusaki, Y., 2004, "Response of Time-Delayed Flowfield Structure behind an Active Vortex Generators Pair," AIAA Paper 04-0427, 36th AIAA Aerospace Sciences Meeting & Exhibit.

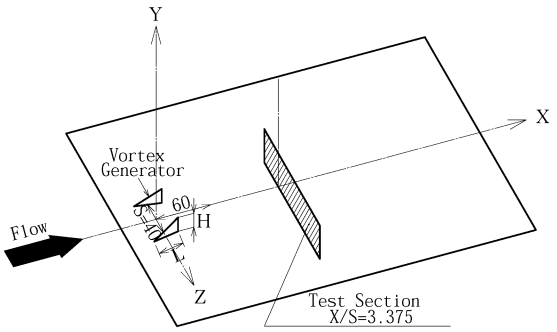

Fig 1 Test section

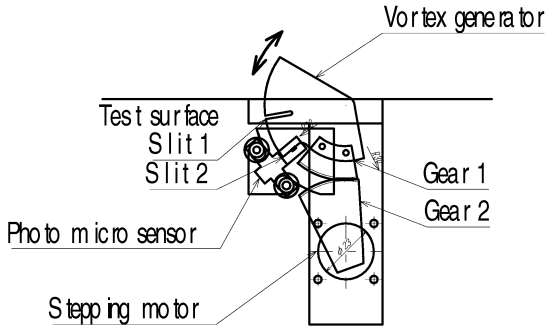

Fig 2 Active vortex generator

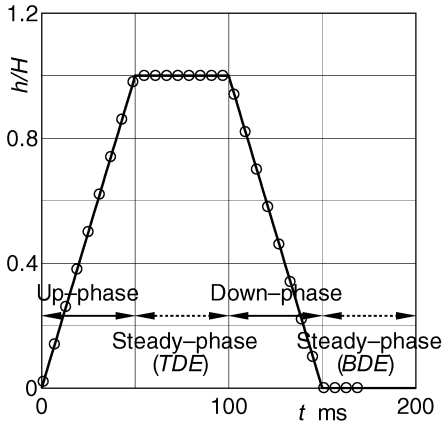

(○ : Time of conditional averaged)

Fig. 3 Timing chart of *AVG* and each phase period

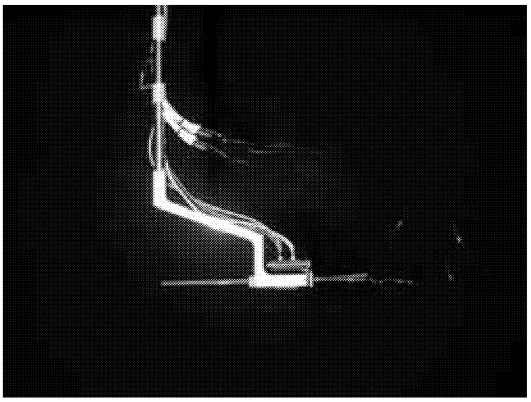

Fig 4 Rotating *X*-array hot-wire sensor

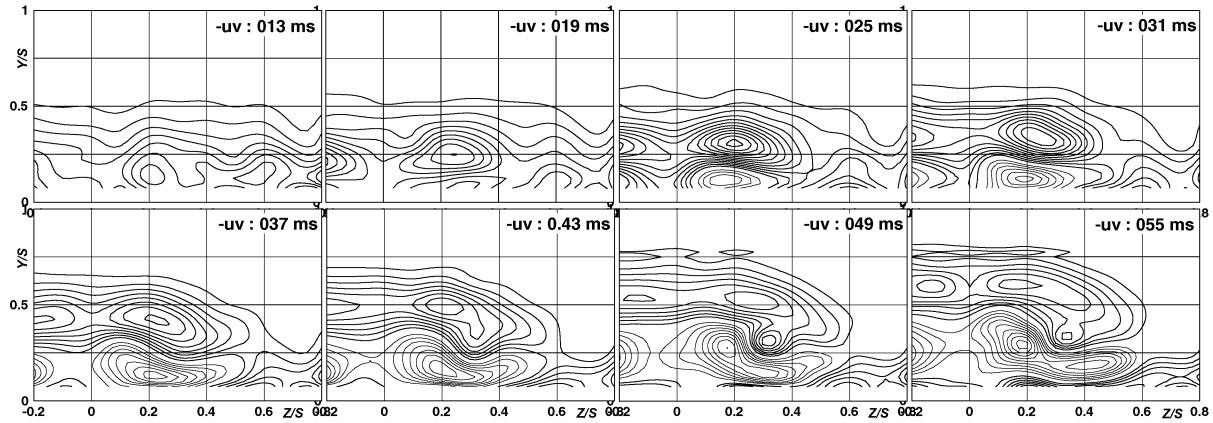

(a) Final-stage of up-phase

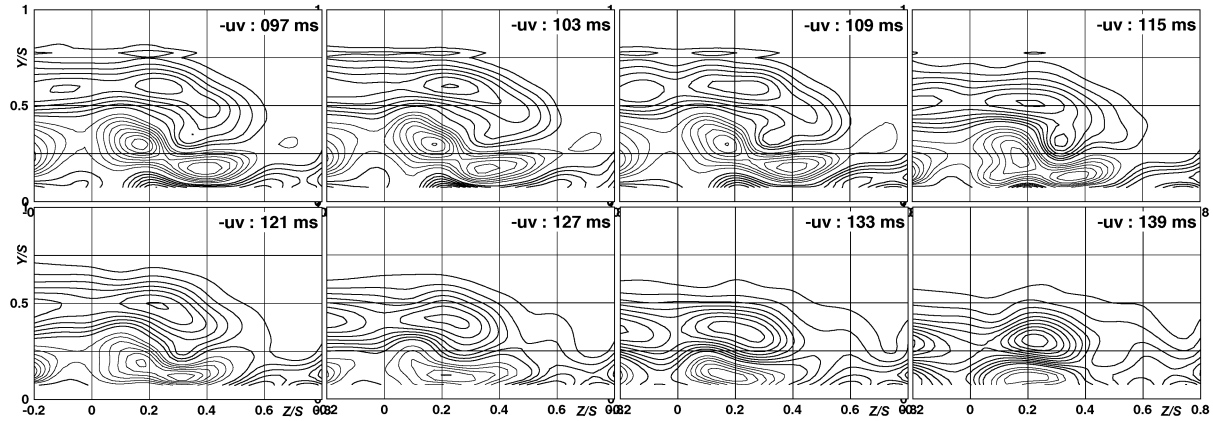

(b) Early-stage of down-phase

Fig.5 Contours of Reynolds shear stress $-\overline{u'v'}/u_{ref}^2$ (outer contour: ±2.5 x 10^{-4}, step: 2.5 x 10^{-4})

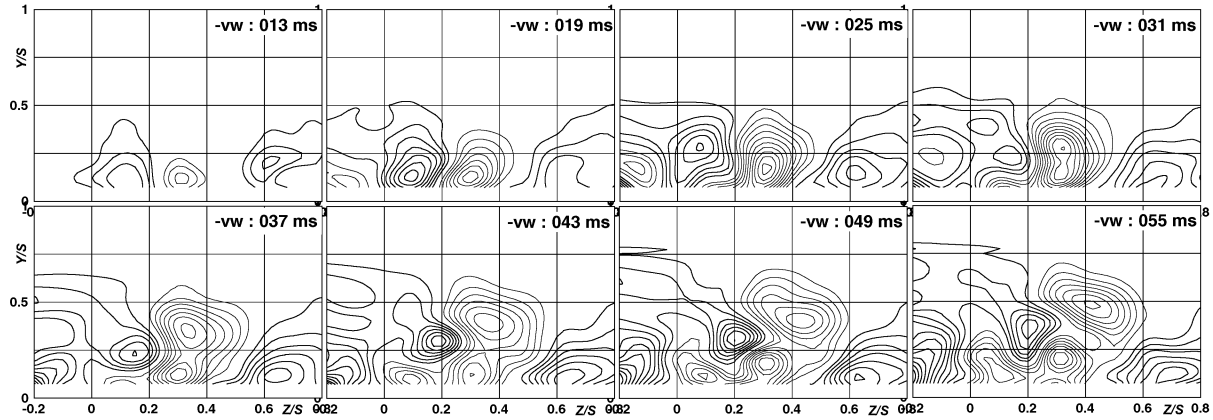

(a) Final-stage of up-phase

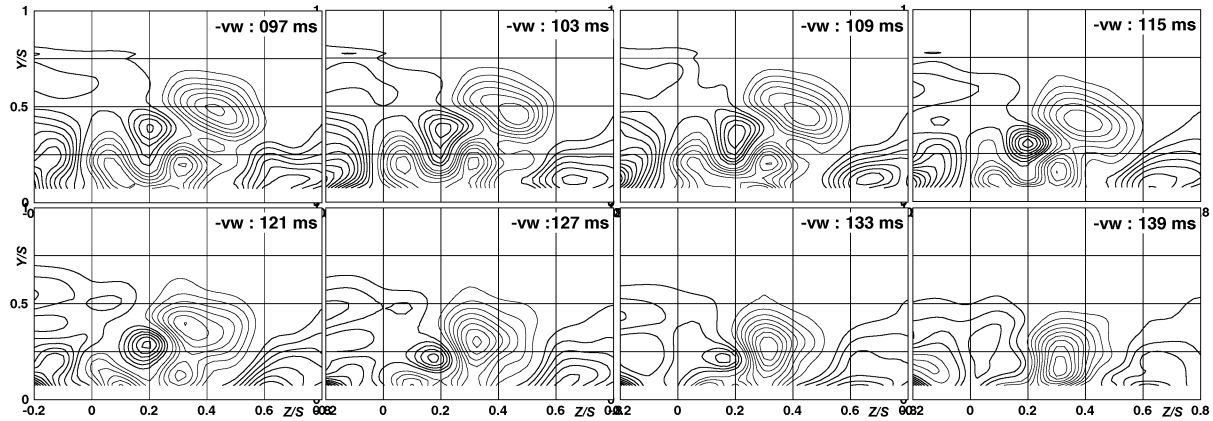

(b) Early-stage of down-phase

Fig.6 Contours of Reynolds shear stress $-\overline{v'w'}/u_{ref}^2$ (outer contour: ±2.5 x 10^{-4}, step: 2.5 x 10^{-4})

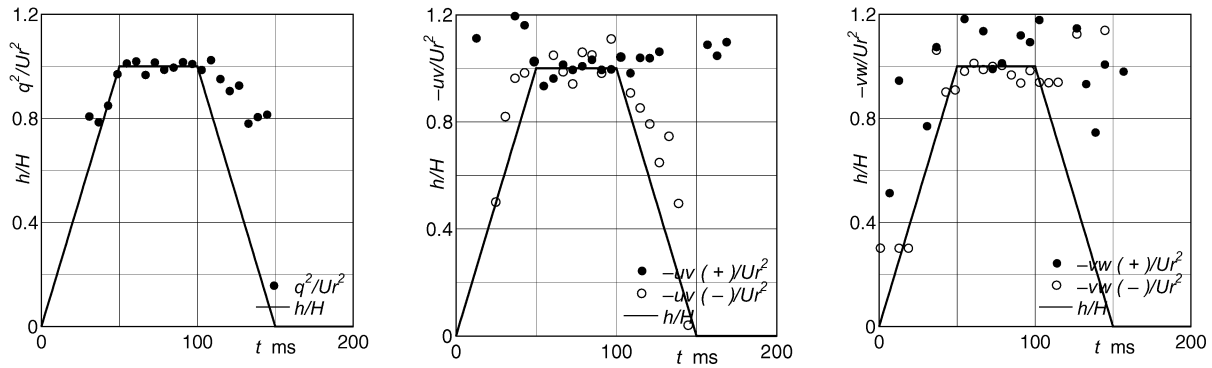

(a) Kinetic energy q^2 (b) Shear stress $-\overline{u'v'}$ (c) Shear stress $-\overline{v'w'}$

Fig 7 Response of turbulent properties normalized by the value at steady-phase to the height of *AVG*

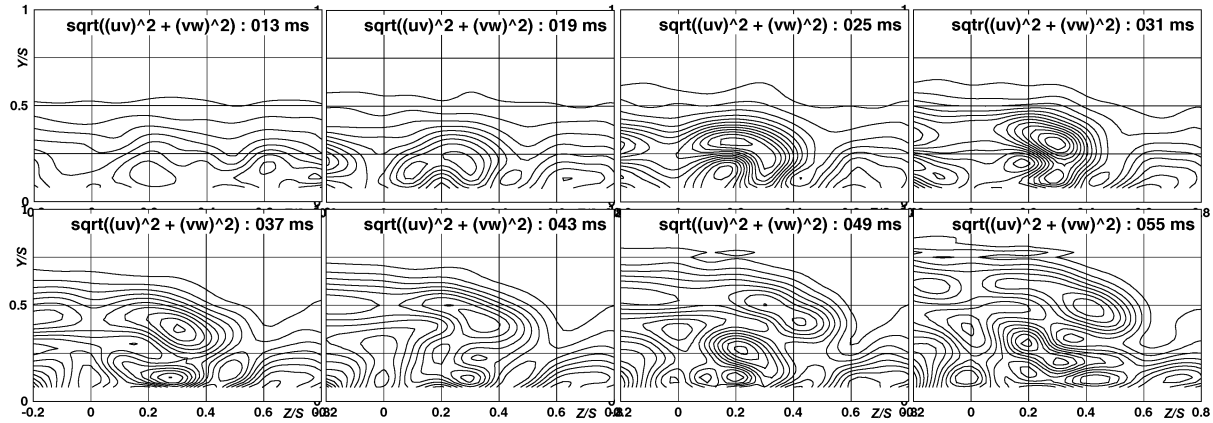

Fig.8 Total stress $\tau = \sqrt{\overline{u'v'}^2 + \overline{v'w'}^2}$ at final-stage of up-phase (outer contour: 2.5 x 10^{-4}, step: 2.5 x 10^{-4})

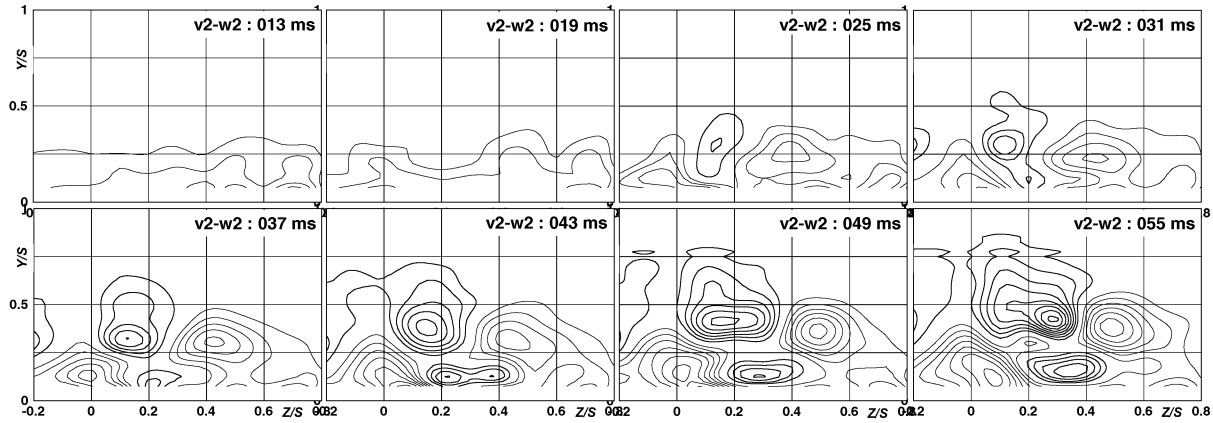

Fig.9 Normal stress anisotropy $\overline{v'^2} - \overline{w'^2}$ at final-stage of up-phase (outer contour: ±5.0 x 10^{-4}, step: 5.0 x 10^{-4})

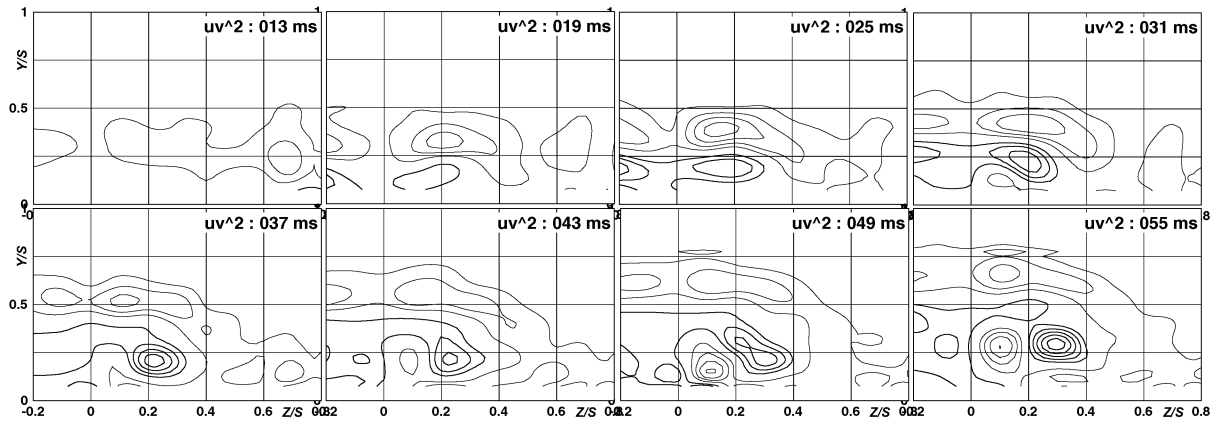

Fig.10 Triple-product $\overline{u'v'^2}/Ur^3$ at final-stage of up-phase (outer contour: ±2.5 x 10^{-5}, step: 2.5 x 10^{-5})

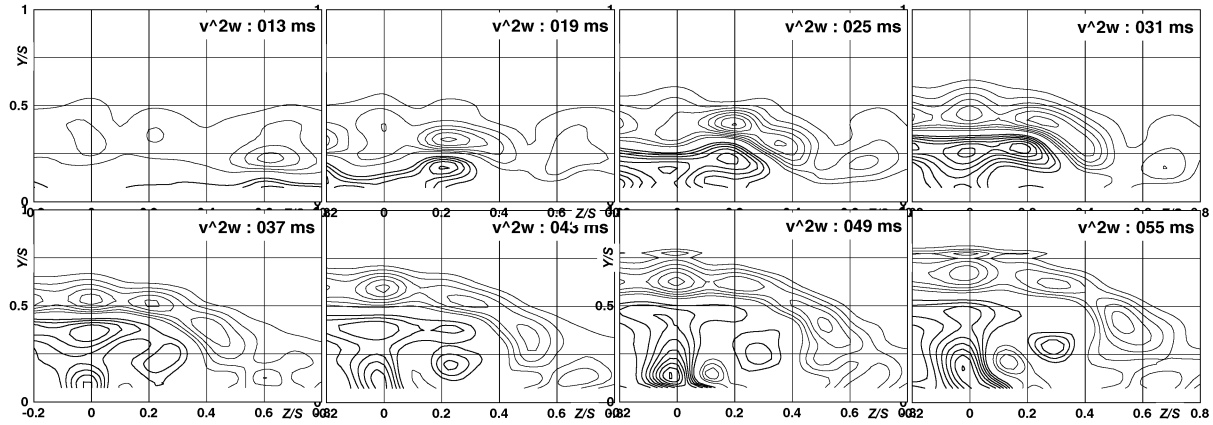

Fig.11 Triple-product $\overline{v'^2 w'}/Ur^3$ at final-stage of up-phase (outer contour: ±5.0 x 10^{-5}, step: 5.0 x 10^{-5})